Monotonic Increase of Nitrite Yields in the Photolysis of Nitrate in Ice and Water between 238 and 294 K

Yael Dubowski, A. J. Colussi,* Christopher Boxe, and M. R. Hoffmann*

*W. M. Keck Laboratories, California Institute of Technology, Pasadena, California 91125*

The quantum yield, ϕ, of nitrite formation in the 302 nm band photolysis of fluid or frozen aqueous nitrate solutions increases monotonically with temperature over the range 238−294 K. The presence of formate increases ϕ 5-fold but does not modify its temperature dependence. Considering that the detection of nitrite as a product is only possible after the initial photofragments ($NO_2^- + O$) escape the solvent cage and that the diffusivity of ice, D_{ice}, is about 6 orders of magnitude smaller than that of supercooled water, D_{aq}, at the same temperature, we infer that nitrate photodecomposition takes place in similar liquidlike media at all temperatures. We found that the nitrite dispersed into the bulk is subsequently degraded by OH radicals, another primary photoproduct that can be scavenged by formate. The fact that experimental ϕ values in ice are actually larger than those derived from linear ϕ vs $D_{aq}T^{1/2}$ extrapolation of aqueous phase data, as expected for cage processes in homogeneous media, suggests that the photochemically relevant properties of the quasi-liquid layer covering ice below the normal melting point resemble those of bulk supercooled water, but other effects, such as the dissipation of excess photon energy into the medium, may also play a role.

Introduction

The photodecomposition of NO_3^- into OH radicals and NO_x species within and upon ice may be crucial to the chemistry of snowpacks and to the composition of the atmospheric boundary layer.[1−6] Nitrogen oxides are released in the process, while OH radicals may initiate the oxidation of organic contaminants in snow and ice.

The ionic content of snow varies from less than 10 μM in pristine areas to the millimolar range in areas affected by anthropogenic deposition.[7] At the temperatures prevalent during spring and summer at mid- and high latitudes, the rejected solutes are expected to reside within the quasi-liquid layer (QLL) present at the ice−air interface and between adjacent ice crystals.[2,3,7] The issue is whether the photodecomposition of nitrate in the QLL is qualitatively or quantitatively different from that occurring in aqueous solutions (reactions 1 and 2). The medium may influence the extent of reactions 1 and 2 by affecting, *inter alia*, the competition between the recombination and dispersal of primary fragments. The separation of geminally produced species is ultimately controlled by the transport properties of the surrounding fluid:

$$NO_3^- + H^+ + h\nu \rightarrow NO_2 + OH \qquad (1)$$

$$NO_3^- + h\nu \rightarrow NO_2^- + O\ (^3P) \qquad (2)$$
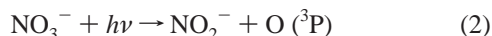
The nature of the QLL has been the subject of recent theoretical[8,9] and experimental studies.[7,10−13] Most of these studies confirmed the presence of a QLL on ice surfaces, but neither its domain of existence nor its thickness and physicochemical properties were firmly established. Wei and co-workers[12,13] showed that the disordering of the surface of hexagonal ice (using sum-frequency vibrational spectroscopy to measure the orientational order of dangling OH bonds) becomes detectable at 200 K and increases dramatically with

temperature. However, even at temperatures close to the normal melting point, the QLL remains structurally different from bulk water. The diffusion coefficient of water in the QLL formed by interfacial melting of ice on graphite and polystyrene[14−16] is similar to its value in the supercooled state. Both experimental work[7,11] and theoretical studies[8] have shown that the thickness of the QLL increases with temperature and ionic strength and under most conditions is thicker than predicted by bulk freezing-point depression.

To confirm that the photodecomposition of nitrate as a solute in ice takes place in the QLL and to explore the photochemically relevant properties of this reaction medium, we now report nitrite formation rates during the photolysis of nitrate in ice pellets and aqueous solutions as a function of temperature.

Experimental Methods

Solutions of 10 mM $NaNO_3$ or 1 mM $NaNO_3$/10 mM $NaCO_2H$ in Milli-Q water were flash-frozen by spraying them into an alumina mortar filled with liquid nitrogen. The granulated solid obtained was then ground in situ into a powder with a pestle while at 77 K. The resulting pulverized ice was then made into cylindrical (13 mm diameter × 4 mm thickness) polycrystalline ice pellets ($\rho \sim 0.9$ g/cm^3) in a French press under an applied pressure of 3.8 MPa. After annealing for about an hour at the desired experimental temperature under ambient pressure (0.1 MPa), the ice pellets were irradiated with light at a wavelength of 313 ± 10 nm. The collimated output of a high-pressure 1000 W Hg−Xe arc lamp was used as a light source in combination with a 320 nm band filter (Melles Griot, UG 11) and a solution of 1 mM potassium chromate in 2.3% potassium carbonate contained in a 1-cm quartz cell. The incident light flux, $I_0 = (2.4 \pm 0.2) \times 10^{16}$ photons cm^{-2} s^{-1}, was measured with potassium ferrioxalate as actinometer.[17] Light absorbance by the nitrate in the pellets before irradiation was determined in a UV−vis spectrophotometer (Shimadzu UV-
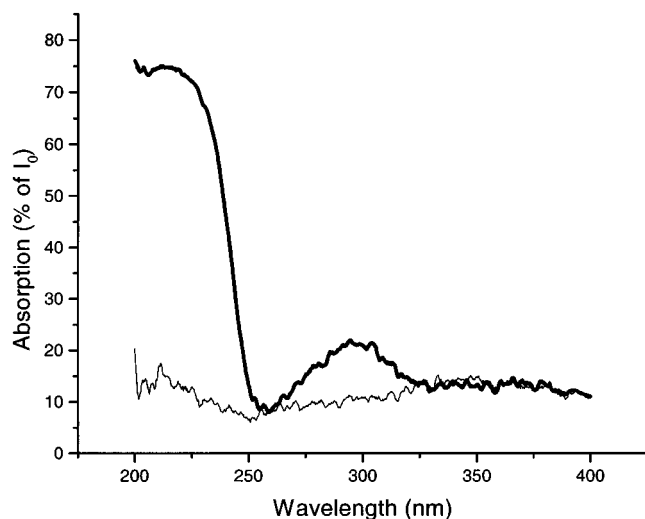
Figure 1. Absorption spectra of 10 mM $NaNO_3$ ice pellets (thick line) and pure ice pellets (thin line). Pellets were 4 mm thick.

2101 PC) with an attached integrating sphere (Shimadzu ISR-260). The technique was explained in detail previously[18] and only a brief description will be given here. The fraction of light transmitted to the pellets, T, was measured by a photomultiplier in line with the incident light beam located at the bottom of the integrating sphere, with air as reference. The fraction of light reflected by the pellets, R, was measured off ice pellets held in a slot, flush with the wall of the integrating sphere, from pelletized $BaSO_4$ powder as reference. The absorption spectra of 10 mM nitrate in ice pellets obtained from these measurements are shown in Figure 1.

During the photochemical experiments, a single ice pellet was snugly lodged inside a circular slot machined in the top face of a cylindrical copper block and was irradiated from above. Temperature control of the copper block and the implanted pellet was provided by coolant circulation from a cryostat (Neslab ULT-80) and monitored by a chromium–aluminum thermocouple (Omega Engineering) attached to the block surface by a frozen water droplet. After irradiation, the pellets were thawed and analyzed colorimetrically for nitrite by use of the Saltzmann reagent.[19]

Results and Discussion

The temporal evolution of nitrite formed by 313 nm photolysis of 10 mM nitrate ice pellets at 253 and 268 K in the absence of formate as radical scavenger is shown in Figure 2. Nitrite concentrations initially increase but approach limiting values at long irradiation times, pointing to nitrite destruction in secondary processes, possibly involving photolysis or radical attack. The fact that the limiting nitrite concentration is a markedly increasing function of temperature suggests the occurrence of a chemical rather than a photochemical sink for nitrite having negative temperature dependence. Confirming such presumption, we found that, in the presence of a 10-fold excess of formate as a radical scavenger, the rate of nitrite formation remains constant up to 60 min at 253 K; see Figure 3 (cf. Figure 2).[20] An Arrhenius plot of the initial rate constants k_i for nitrite formation in ice pellets in the presence and absence of formate as radical scavenger is shown in Figure 4. Notice the enhanced rates in the presence of formate and the similar slopes of both sets of experiments.

A direct comparison of the rates of nitrite formation during the irradiation of fluid and frozen nitrate solutions would overlook the inevitable differences of light absorption by nitrate
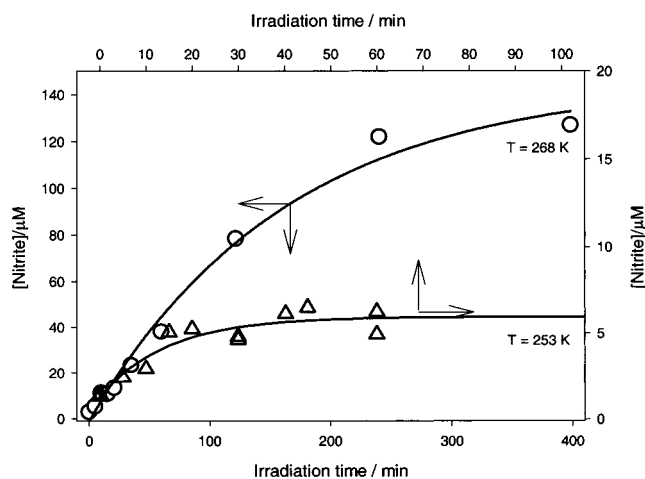
Figure 2. Nitrite concentration as a function of irradiation time in ice pellets made of 10 mM $NaNO_3$ aqueous solutions: ($\triangle$) at 253 K; ($\bigcirc$) at 268 K.
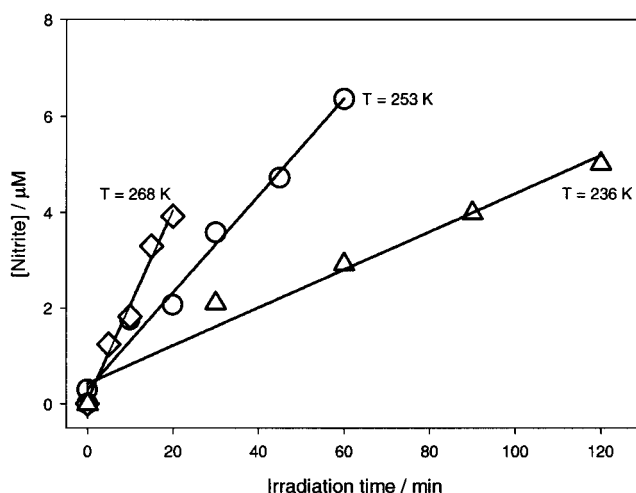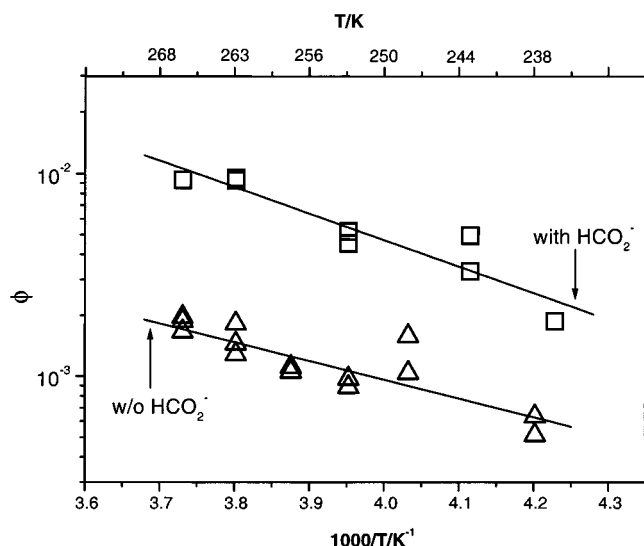

Figure 3. Nitrite concentration as a function of irradiation time in ice pellets made of 1 mM $NaNO_3$ + 10 mM $NaCO_2H$ aqueous solutions at different temperatures: ($\triangle$) 236 K; ($\bigcirc$) 253 K; ($\diamond$) 268 K.
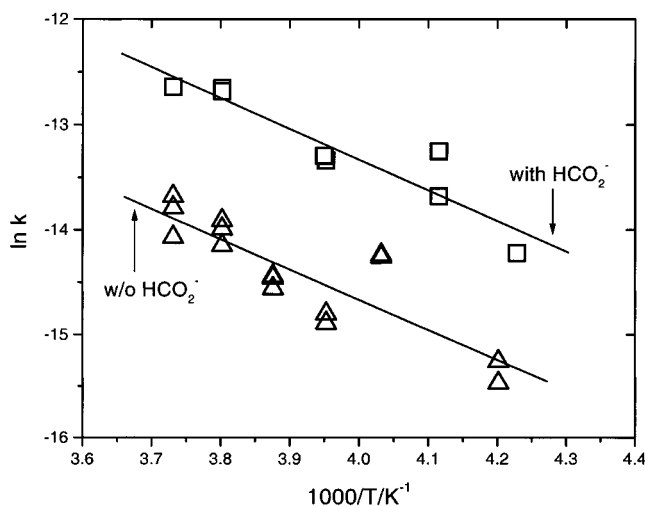
Figure 4. Natural logarithm of the initial rate constants of nitrite production during the 313 nm irradiation of nitrate-doped ice pellets vs $1000/T$ (in kelvins): ($\triangle$) 10 mM $NaNO_3$; ($\square$) 1 mM $NaNO_3$ + 10 mM $NaCO_2H$.

in both cases. Thus, a meaningful test of medium effects involves comparing quantum yields in the two phases. The fraction of incident light ($\lambda = 313$ nm) absorbed by nitrate as

Increased Nitrite Yields in Nitrate Photolysis

J. Phys. Chem. A, Vol. 106, No. 30, 2002 **6969**

Figure 5. Natural logarithm of the quantum yields $\phi_{NO_2^-}$ for the experiments of Figure 4 vs $1000/T$ (in kelvins).

Figure 6. Quantum yields of nitrite formation $\phi_{NO_2^-}$ vs $1000/T$ (in kelvins) in 10 mM NaNO₃ aqueous solutions (○) and in ice pellets made of the same solutions (◇).

present in ice pellets was evaluated from I_0, T, and R data (see above):

$$\frac{I_a}{I_0}\Big|_\lambda = \{(100 - T - R)_{\lambda, NO_3^-, ice} - (100 - T - R)_{\lambda, H_2O, ice}\} \tag{3}$$

where I_a/I_0 is the percentage of incident light absorbed by NO_3^- in an ice pellet (I_a = absorbed light flux, I_0 = incident light flux), $(100 - T - R)_{\lambda, NO_3^-, ice}$ is the percentage of light absorption by an ice pellet containing NO_3^-, and $(100 - T - R)_{\lambda, H_2O, ice}$ is the percentage of light absorption by a pure H_2O ice pellet (T = % light transmitted through the ice pellet, R = % light reflection from the ice pellet). We found that, as in the case of aqueous solutions, the UV absorption spectrum of nitrate in ice pellets shows two absorption bands at about 200 and 300 nm. The use of eq 3 leads, for example, to $I_a/I_0 = (5.4 \pm 1.3)\%$ for 10 mM nitrate.

The quantum yields ϕ for the formation of NO_2^- were calculated as follows:

$$\phi = \left(\frac{d[NO_2^-]}{dt}\right)_0 \frac{V}{R_a} \tag{4}$$

where $(d[NO_2^-]/dt)_0$ is the initial rate of nitrite formation (in moles per liter per second), V is the volume of the irradiated ice pellet (in liters), and R_a represents the photon rate absorbed by nitrate within the pellets (in moles per second). The latter was calculated from the measured incident photon flux I_0, the pellet cross section $S = 1.327$ cm², and the fraction of incident light absorbed by nitrate in the pellet (I_a/I_0) as given by eq 3: $R_a = I_0(I_a/I_0)S$. The low absorbance of 1 mM nitrate at 313 nm precluded a direct measurement. Thus, we assumed the validity of the Beer−Lambert law down to 1 mM, i.e., $(I_a/I_0)_{1\ mM\ NO_3^-} = 0.1(I_a/I_0)_{10\ mM\ NO_3^-}$. The derived quantum yields vary from 5 × 10⁻⁴ to 1 × 10⁻² as a function of temperature and the presence of formate (Figure 5). In all cases, ϕ decreases with decreasing temperature. At constant temperature, quantum yields increase by a factor of ∼5 in the presence of formate but are nearly independent of nitrate concentration between 1 and 10 mM. A $\ln \phi$ vs $1000/T$ plot of data obtained in fluid and frozen 10 mM nitrate solutions is shown in Figure 6. It is apparent that ϕ does not follow linear Arrhenius behavior across the entire
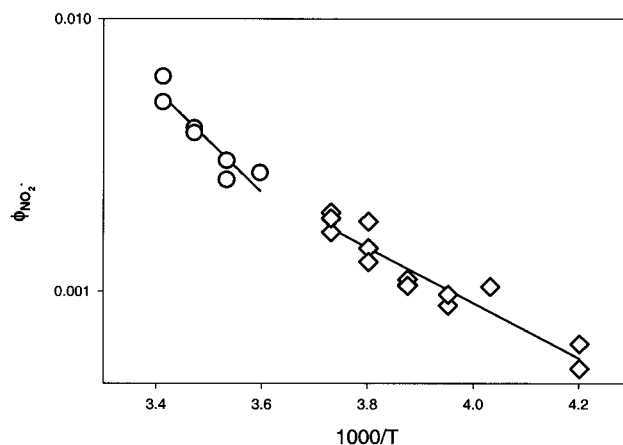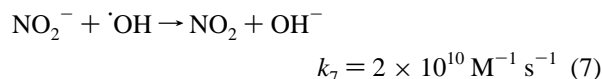
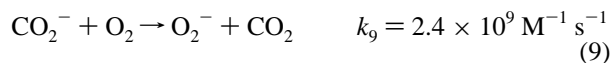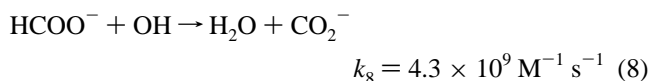temperature range, displaying a perceptible but gentle inflection about the normal melting point.

The above observations are consistent with previous information. The $\lambda > 300$ nm photolysis of nitrate in aerated aqueous solutions at pH < 6 is known to proceed via two primary pathways, reactions 1 and 2. In the absence of radical scavengers, nitrite is formed directly via reaction 2 and, to some extent, via reaction 5:

$$NO_3^- + O\,(^3P) \rightarrow NO_2^- + O_2 \qquad k_5 = 2 \times 10^8\ M^{-1}\ s^{-1} \tag{5}$$
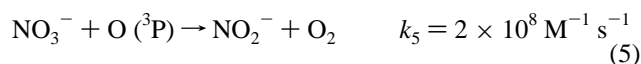
The nitrite thus produced ($\epsilon_{max} = 22.5\ M^{-1}\ cm^{-1}$ at 360 nm) undergoes secondary photolysis, step 6, and oxidation by the OH radicals generated in reaction 1, step 7:

$$NO_2^- + H^+ + h\nu \rightarrow NO + {}^{\cdot}OH \tag{6}$$

$$NO_2^- + {}^{\cdot}OH \rightarrow NO_2 + OH^- \qquad k_7 = 2 \times 10^{10}\ M^{-1}\ s^{-1} \tag{7}$$

The presence of HCO_2^-, which is an efficient OH radical scavenger, would not only prevent nitrite losses via reaction 7 but actually convert nitrogen dioxide, the major product of nitrate photolysis, into additional nitrite via reactions 8−10:

$$HCOO^- + OH \rightarrow H_2O + CO_2^- \qquad k_8 = 4.3 \times 10^9\ M^{-1}\ s^{-1} \tag{8}$$

$$CO_2^- + O_2 \rightarrow O_2^- + CO_2 \qquad k_9 = 2.4 \times 10^9\ M^{-1}\ s^{-1} \tag{9}$$

$$O_2^- + NO_2 \rightarrow O_2 + NO_2^- \tag{10}$$

Therefore, at steady state in the absence of formate

$$\frac{d[NO_2^-]}{dt} = \phi_2 I_{a, NO_3^-} + k_5[O]_{ss}[NO_3^-] - \phi_6 I_{a, NO_2^-} - k_7[OH]_{ss}[NO_2^-] \tag{11}$$

where $[O]_{ss}$ and $[OH]_{ss}$ are the steady-state concentrations of these species in the fluid volume where the reactions actually take place. Considering that $[NO_2^-]$ becomes a linearly increasing function of time upon formate addition (Figure 3), photochemical nitrite losses must be relatively minor, i.e.,
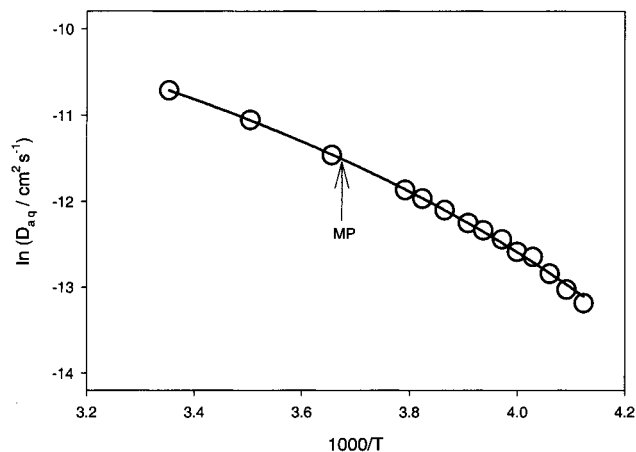
Figure 7. Natural logarithm of water or supercooled water diffusivity D_{aq} vs $1000/T$ (in kelvins). Data are from ref 26. The solid curve corresponds to $D_{aq} = (5.05 \times 10^{-4})\exp[399/T - 170)]$ cm^2 s^{-1}.

Figure 8. $\phi_{NO_2^-}$ in 10 mM NaNO$_3$ aqueous solutions (○) and in ice pellets (◇) vs $D_{aq}T^{1/2}$.

$k_7[OH]_{ss}[NO_2^-] > \phi_6 I_{a,NO_2^-}$ under present conditions. Thus, the limiting concentration of nitrite will be given by

$$[NO_2^-]_{ss} \approx \frac{\phi_2 I_{a,NO_3^-}}{k_7[OH]_{ss}} \quad (12)$$

Since the steady-state concentration of nitrite reached in the absence of formate is positively correlated with temperature,[21] the rate of nitrite production must increase and/or its destruction rate must decrease with temperature. The fact that initial rates of nitrite formation in ice pellets, which are proportional to $\phi_2 I_{a,NO_3^-}$, increase with temperature (see above) and that a similar dependence is expected for k_7 (see below) implies that the steady-state concentration of the photochemically generated OH radicals in the accessible reaction medium should markedly decrease with increasing temperature. This phenomenon is to be expected if the medium were the thicker QLL that develops at higher temperatures.[11,22]

Further analysis of the quantum yields (Figure 6), above and below the melting point, would begin by provisionally assuming, based on the lack of a break at the melting point, that the reaction medium is liquidlike under all conditions. The temperature dependence of the quantum yields of photofragmentation reactions in condensed media has been generally analyzed by means of a continuum hydrodynamic model for the escape of the reactive photofragments from the solvent cage. It has been shown that the probability that two geminate fragments will eventually recombine is proportional to $[1 - (A/\alpha)T^{1/2} \eta^{-1}]$, where A is a constant that depends on the fragments masses and radii, α is the probability of their combination in each collision, and η is the macroscopic viscosity of the medium.[23-25] Since the viscosity is inversely proportional to the diffusivity of the medium D, the net probability of escape from the cage or, what is equivalent in this case, the temperature dependence of the quantum yield ϕ of the nitrite detectable in the bulk, could be represented as

$$\phi = a + bDT^{1/2} \quad (13)$$

where a and b are temperature-independent parameters. The diffusivity of water and supercooled water D_{aq} down to -31 °C, which follows the empirical Vogel−Fulcher−Tammann equation, $D_{aq} = (5.05 \times 10^{-4})\exp[399/(T - 170)]$,[26,27] is plotted in Figure 7. The fact that the data obtained in aqueous and ice phases are not aligned in the plot $\phi_{nitrite}$ vs $D_{aq}T^{1/2}$ shown in Figure 8 is an indication that the diffusivity of bulk supercooled
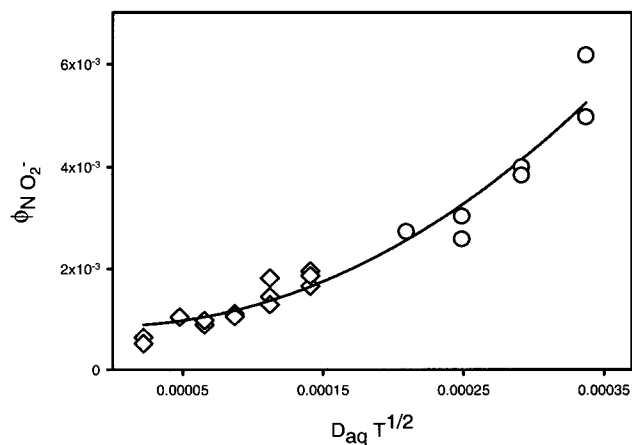
water does not adequately represent the photochemically relevant transport properties of the QLL. It should be emphasized that since the diffusivity of crystalline ice is about 6 orders of magnitude smaller than D_{aq} over the same temperature range, ϕ should have dropped accordingly below the normal melting point, at variance with observations.

The question arises whether the observed curvature in Figure 8 is the result of the decreasing thickness of the QLL as temperature drops or whether there is an additional effect due to changes in the nature of the QLL with temperature. The fact that the quantum yield, ϕ, for nitrite formation in ice increases in the presence of formate as an OH scavenger (Figure 5) suggests the occurrence of reaction 7, as well as reactions 8−10, taking place in a common fluid environment where all solutes could compete for OH radicals. Thus, we measured $\phi \approx 9 \times 10^{-3}$ at 268 K in ice pellets containing formate. Extrapolation of this value to higher temperatures on the basis of Figure 8 gives $\phi \sim 0.02$ at 298 K, which is within a factor of 2 of the ϕ value measured during the photolysis of aqueous NaNO$_3$ solutions in the presence of formate at $\lambda = 305$ nm, 298 K.[28]

The quantum yield, $\phi = (1.5 \pm 0.3) \times 10^{-3}$, obtained in ice pellets doped with 10 mM NaNO$_3$ at 263 K, is in essential agreement with the $\phi = (4.8 \pm 1.5) \times 10^{-3}$ value we previously determined during the photolysis of submillimeter ice films obtained by spraying KNO$_3$ solutions on a cold surface.[21] The difference between these quantum yields may be the result of the substantially different protocols used in the two sets of experiments and underscores the role of morphology on quantitative ice photochemistry. Nitrate, like most other solutes, is expected to be excluded from the ice matrix during freezing and to accumulate in the QLL at the surface of ice crystals and between adjacent crystals.[29] However, under the fast freezing conditions in the present study, only partial exclusion from the ice matrix is expected.[30]

The continuity of the quantum yields for nitrite formation in aqueous solution and in ice pellets around the melting point confirms that NO$_3^-$ photolysis occurs in a liquidlike environment, most likely the QLL covering ice well below freezing, under all conditions. This conclusion is in accord with interfacial melting experiments of ice against graphite and polystyrene, showing that diffusion coefficient of the QLL is approximately equal to that of supercooled water.[14-16,31] However, the nonlinear temperature dependence of ϕ on $D_{aq}T^{1/2}$, leading to ϕ values in ice that are larger than extrapolated aqueous phase data, suggests that the escape of primary photochemical fragments from the solvent cage in the QLL is faster than expected

on the basis of bulk diffusivities. Since the excess photon energy generated in reaction 2 into the surrounding medium [$h\nu$(310 nm) $- \Delta H_2 \sim (92 - 75) = 17$ kcal/mol] is enough to melt about 12 ice water molecules, or heat a considerable volume of the QLL several degrees, it should certainly affect the probability of escape, at least to a different extent than in the bulk fluid. However, the fact that the steady-state concentration of nitrite, which is largely determined by reaction 7, i.e., by reaction with OH radicals, increases with temperature supports the view that the positive temperature dependence of the thickness of the QLL, which is inversely proportional to [OH] (vide supra eq 12), is the leading factor controlling ϕ in ice.

References and Notes

(1) Honrath, R. E.; Peterson, M. C.; Guo, S.; Dibb, J. E.; Shepson, P. B.; Campbell, B. *Geophys. Res. Lett.* **1999**, *26*, 695−698.

(2) Honrath, R. E.; Peterson, M. C.; Dziobak, M. P.; Green, S.; Dibb, J. E.; Arsenault, M. A. *Geophys. Res. Lett.* **2000**, *27*, 2237−2240.

(3) Honrath, R. E.; Guo, S.; Peterson, M. C.; Dziobak, M. P.; Dibb, J. E.; Arsenault, M. A. *J. Geophys. Res.* **2000**, *105*, 24183−24190.

(4) Jones, A. E.; Weller, R.; Minikin, A.; Wolff, E. W.; Stuges, W. T.; McIntyre, H. P.; Leonard, S. R.; Schrems, O.; Bauguitte, S. *J. Geophys. Res.* **1999**, *104*, 21355−21366.

(5) Jones, A. E.; Weller, R.; Wolff, E. W.; Jacobi, H.-W. *Geophys. Res. Lett.* **2000**, *27*, 345−348.

(6) Ridley, B.; Walega, J.; Montzka, D.; Grahek, F.; Atlas, E.; Flocke, F.; Stroud, V.; Deary, J.; Gallant, A.; Boudries, H.; Bottenheim, J.; Anlauf, K.; Worthy, D.; Sumner, A. l.; Splawn, B.; Shepson, P. *J. Atmos. Chem.* **2000**, *36*, 1−22.

(7) Conklin, M.; Bales, R. C. *J. Geophys. Res.* **1993**, *98*, 16851−16855.

(8) Wettlaufer, J. S. *Phys. Rev. Lett.* **1999**, *82*, 2516−2519.

(9) Bolton, K.; Pettersson, J. B. C. *J. Phys. Chem. B* **2000**, *104*, 1590−1595.

(10) Doppenschmidt, A.; Kappl, M.; Butt, H.-J. *J. Phys. Chem. B* **1998**, *102*, 7813−7819.

(11) Doppenschmidt, A.; Butt, H.-J. *Langmuir* **2000**, *16*, 6709−6714.

(12) Wei, X.; Shen, Y. R. *Abstr. Pap. Am. Chem. Soc.* **2000**, *220*, U162−U162.

(13) Wei, X.; Miranda, P. B.; Shen, Y. R. *Phys. Rev. Lett.* **2001**, *86*, 1554−1557.

(14) Maruyama, M.; Bienfait, M.; Dash, J. G.; Coddens, G. *J. Crystal Growth* **1992**, *118*, 33−40.

(15) Gay, J. M.; Suzanne, J.; Dash, J. G.; Fu, H. Y. *J. Crystal Growth* **1992**, *125*, 33−41.

(16) Fu, H. Y.; Dash, J. G. *J. Colloid Interface Sci.* **1993**, *159*, 343−348.

(17) Hatchard, C. G.; Parker, C. A. *Proc. R. Soc., Ser. A.* **1956**, *235*, 518.

(18) Dubowski, Y.; Hoffmann, M. R. *Geophys. Res. Lett.* **2000**, *27*, 3321−3324.

(19) Saltzmann, B. E. *Anal. Chem.* **1954**, *26*, 1949−1955.

(20) Mark, G.; Korth, H. G.; Schuchmann, H. P.; von Sonntag, C. *J. Photochem. Photobiol. A: Chem.* **1996**, *101*, 89−103.

(21) Dubowski, Y.; Colussi, A. J.; Hoffmann, M. R. *J. Phys. Chem. A* **2001**, *105*, 4928.

(22) Sadtchenko, V.; Giese, C.; Gentry, W. *J. Phys. Chem. B* **2000**, *104*, 9421−9429.

(23) Noyes, R. M. *Prog. Reaction Kinetics* **1961**, *1*, 129.

(24) Ghibaudi, E.; Colussi, A. J. *Chem. Phys. Lett.* **1983**, *94*, 121.

(25) *Free Radicals*; Koenig, T., Fischer, H., Kochi, J., Eds.; Wiley: New York, 1973; Vol. 1, Chapt. 4.

(26) Gillen, K. T.; Douglass, D. C.; Hoch, M. J. R. *J. Chem. Phys.* **1972**, *57*, 5117.

(27) Smith, R. S.; Kay, B. D. *Nature* **1999**, *398*, 788.

(28) Warneck, P.; Wurzinger, C. *J. Phys. Chem.* **1988**, *92*, 6278−6283.

(29) Killawee, J. A.; Fairchild, I. J.; Tison, J. L.; Janssens, L.; Lorrain, R. *Geochim. Cosmochim. Acta* **1998**, *62*, 3637.

(30) van der Ham, F.; Witkamp, G.; de Graauw, J.; van Rosmalen, G. *J. Crystal Growth* **1999**, *199*, 744−748.

(31) Dash, J. G.; Fu, H. Y.; Wettlaufer, J. S. *Rep. Prog. Phys.* **1995**, *58*, 115−167.